Struct Multidisc Optim 24, 60–71 © Springer-Verlag 2002
Digital Object Identifier (DOI) 10.1007/s00158-002-0214-2

Efficient optimization of a noise transfer function by modification of a shell structure geometry – Part II: Application to a vehicle dashboard*

S. Marburg and H.-J. Hardtke

Abstract The subject of the second part of this paper is the application of the method presented and discussed in Part I. In particular, the concept of component models is briefly sketched. This is followed by a description of the computational model. The symmetry half of a sedan dashboard consists of finite shell elements, whereas the remaining body structure is represented by one superelement. The fluid model consists of boundary elements. The noise transfer function is calculated next. Six possible objective functions are presented. Further, the effect of fictitious stiffening is investigated, to find out if a stiffening decreases radiated noise. The description of the large number of 44 parameters is followed by the discussion of the optimization result. Only by modifying the shell structure geometry by $\pm$ 10 mm, an average improvement of three decibel is achieved for this model. Finally, the result as well as the entire process are critically reviewed and discussed.

Key words structural acoustics, noise transfer function, sound pressure level, acoustic influence coefficients, booming noise, component model, optimal shell geometry, sedan interior noise

1 Introduction

This article is based on the fundamentals of the calculation of the noise transfer function, its valuation and the sensitivity analysis shown in the first part of this paper. The application of the method is facing the so-called booming noise problems in vehicle interior acoustics (cf. Flanigan and Borders 1984; Ishiyama *et al.* 1988; Kitamura *et al.* 1990; Yamazaki and Inoue 1989). Several different definitions on this name are known. However, in many cases booming noise is noise appearing in a frequency range that may be analyzed by using finite element models of the body structure. Owing to a large number of publications on booming noise the upper frequency limit varies between 60 Hz (Flanigan and Borders 1984) and 250 Hz (Kitamura *et al.* 1990). Giebeler and Booz (1994) discussed investigation of analysis of sedan body structures using finite element models in the frequency range even above 250 Hz. However, they further indicate that success of these efforts has been rather poor by now. Herein, the upper limit of the frequency domain is 200 Hz.

Concerning the decrease of noise, in particular vehicle interior noise, several methods were applied. Some trial and error methods are based on simulation techniques. Further, interacting simulation and experimental techniques are reported. As an example, Mühlmeier *et al.* (1994) succeeded in decreasing low frequency noise by stiffening the rear door of a station wagon. Kitamura *et al.* (1990) improved the acoustic characteristics by increasing the windshield mass. They also applied combined simulation and experimental techniques. Hagiwara *et al.* (1991) improved the acoustic behaviour of a vehicle body by the suitable use of modal sensitivities. More recent development of that was including optimization techniques as found in the paper by Pal and Hagiwara (1994).

Remarks on general acoustic optimization are found in papers by Hambric (1995, 1996) Christensen *et al.* (1998), Christensen and Olhoff (1998), and Marburg *et al.* (1997a,b). The papers mentioned above by Hambric and Christensen *et al.* usually cover the optimization of the whole coupled structural acoustic problem. This remark is also valid for Pal and Hagiwara (1994). In contrast to these publications, herein the authors take advantage of the assumption that the acoustic properties do not change if the geometric modifications during the optimization process are much smaller than the acoustic wavelength. In this case, the acoustic boundary value

Received February 2, 2001
Received by Design Optimization September 13, 1999

S. Marburg and H.-J. Hardtke

Institut für Festkörpermechanik, Technische Universität, D–01062 Dresden, Germany
e-mail: marburg@ifkm.mw.tu-dresden.de

* This paper was originally submitted to and accepted by the discontinued journal *Design Optimization*

problem has to be solved only once during the whole optimization process. This is realized by calculation of acoustic influence coefficients. These influence coefficients account for the mapping of the structural particle velocities to the sound pressure at a certain fluid field point. In this paper, the driver's ear is used to represent this field point.

This paper presents the whole process of the optimization of a vehicle panel. It applies the concepts of the first part of this paper. In addition to that, the concept of a component model is discussed and some more practical points will be considered. The latter includes model descriptions and choice of parameters. A study concerning stiffening of the shell structure is added to investigate whether a stiffer structure would decrease the noise transfer function and to compare with optimization results.

It shall be mentioned that a major part of the analysis was carried out by the commercial finite element code ANSYS. This includes parametric modelling, structural and sensitivity analysis and optimization. The acoustic influence coefficients were calculated by the noncommercial boundary element program AKUSTA that has been developed at the Institut für Festkörpermechanik at the Technical University of Dresden.

This paper does not address the problem of creating a realistic sedan body model. The authors were provided with a body structure, with the data that were required to create the component model and with the fluid's surface model of the cabin. This paper should rather be understood to describe the methodology with realistic background. The simulation models of both, the body structure and the fluid, had been applied for industry relevant simulations. The industrial background of these simulations is to find out trends in the early stage of development of body structures. Finally, we mention that the subject of noise level reduction by poroelastic layers is excluded from our considerations. It is noted that these layers can substantially contribute to decrease the interior noise of cars.

2 Concept of a component model

In order to achieve a fast optimization process it is useful to decompose a large structure into single components. The idea is then to have a shell structure for the component under consideration and to reduce the remaining part of the structure to its modal behaviour. That means, we end up with a detailed shell of a certain component and a superelement representing the remaining part of the structure. Nevertheless, to analyze the acoustic properties the whole fluid filled cabin is considered. However, only the parts of the detailed shell structure at the fluid surface contribute to the excitation of the fluid. To justify this simplification we consider (15) of Part I

$$p_i(\omega) = \mathbf{b}^T(\omega)\mathbf{v}_s(\omega)\,. \tag{1}$$

We now leave the symbolic matrix notation and decompose it into sound radiating shell nodes and a nonradiating remaining surface (rigid nodes)

$$p_i = \underbrace{\sum_{j=1}^{\substack{\text{all shell}\\ \text{nodes}}} b_j v_{s_j}}_{\neq 0} + \underbrace{\sum_{k=1}^{\substack{\text{all rigid}\\ \text{nodes}}} b_k v_{s_k}}_{=0}\,. \tag{2}$$

As for the rigid surface the structural particle velocity is zero for the component model and, hence, (2) reduces to the first term on the right-hand side.

In general, one has to expect both positive and negative real and imaginary parts for the nodal contribution to the sound pressure p_i. So it may happen that in case of decreasing the sound pressure due to a single component, the sound pressure due to vibration of the whole structure increases. However, if this procedure of creating a superelement of the remaining structure and decreasing the sound pressure due to the radiation of a vibrating shell is sequentially repeated for different components most likely the sound pressure will be decreased for the whole vibrating structure as well. Obviously, the latter remark does not hold for acoustically optimized or nearly optimized systems.

3 Model description and requirements

According to the previous section the right symmetric half of an entire vehicle body is decomposed into the shell structure of the dashboard and a superelement of the remaining structure. Whereas the dashboard shell consists of about one thousand nodes and bilinear shell elements the degree of freedom of the superelement is 870. It shall be mentioned that the superelement consists of 88 coupling nodes – nodes that appear identically in the shell model – and 60 other nodes. The superelement was created by means of Guyan reduction technique (see, for example Zienkiewicz 1977, Chapt. 20), and provided to the authors. Figure 1 gives an illustration of the dashboard embedded in the vehicle body structure.

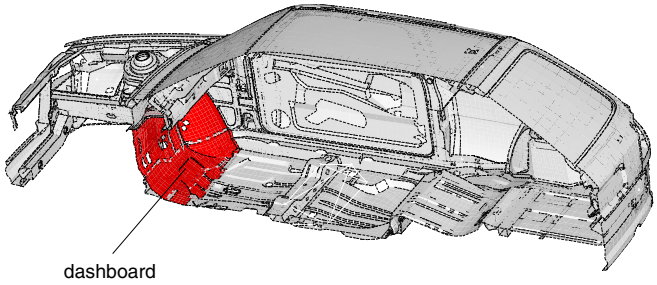

Fig. 1 Dashboard embedded in entire body structure; component model. Dashboard represented by elastic shell, remaining body structure by superelement

It should be explained that only one symmetry half is used for simplification reasons. Furthermore, it had been discovered that – at least for the current model – the symmetric load case provides higher sound pressure levels than the asymmetric excitation. For that reason, only the symmetric case is examined in this paper. The excitation is located at one engine mount: A unit force in vertical direction. Owing to symmetry conditions, the point force applies in the left part as well. The vehicle body appears as a free–free structure, i.e. it is not supported anywhere and has three zero eigenfrequencies.

The fluid boundary element model consists of about 1100 nodes and bilinear elements, Fig. 2. An admittance boundary condition is applied to the fluid surface. As in the paper by Marburg *et al.* (1997a) a homogeneously distributed admittance value of

$$Y = \frac{f}{f_0}\frac{1}{\rho c}\,, \qquad f_0 = 2800\,\mathrm{Hz} \tag{3}$$

is used. There f is the frequency, ρ and c the fluid density and speed of sound. This boundary admittance is subject to experimental determination of the reverberation time. For further discussion of this we refer to Marburg and Hardtke (1999).

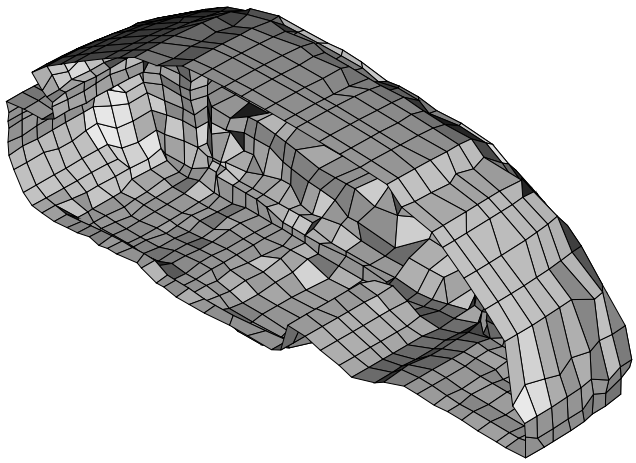

Fig. 2 Symmetry half of fluid boundary element model

As a constraint, coupling points must not be modified during the optimization process. They represent welding points, indicated as bearings in the finite element model of the original structure, Fig. 3.

In the following, we distinguish between the *original* model, the *initial* model and the *optimum*. The *original* model is the model that was provided for optimization. The *initial* model is a geometry based model reconstructed from the *original*. The *initial* model is in a certain sense a homogenized variant of the *original* model since a few details such as the beads in the domain above the welding points in the left part are removed. Further, we will call the model to be yielded via optimization the *optimum*.

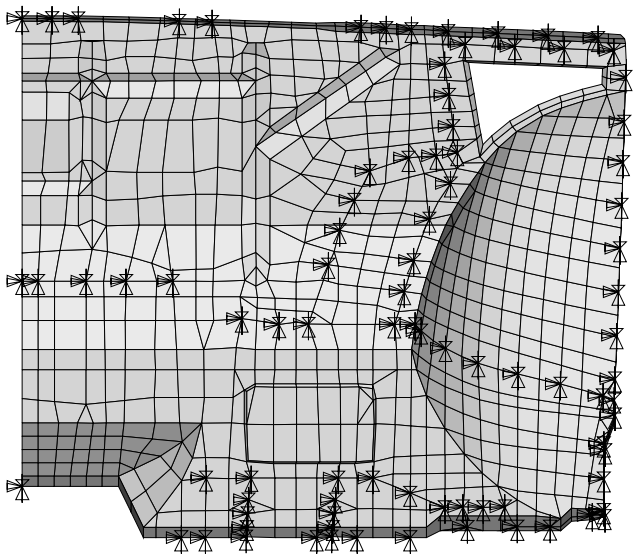

Fig. 3 Finite element model of *original* dashboard (symmetry half), welding points indicated as bearings, view from the right hand front seat

4
Calculation of the noise transfer function

Because the excitation of the model is symmetric, only symmetric modes and load cases of the structure were taken into account. However, though the cabin surface is symmetric the influence coefficients on the right-hand side of the car are different from those on the left-hand side. This is due to the position of the drivers ear as the driver is not sitting in the symmetry plane. We assume the driver sitting on the left front seat.

The modal behaviour of the complete model is characterized by the expected three rigid body modes. Elastic vibration modes are found below 20 Hz. However, they result from other parts of the body. Global mode shapes may occur from about 30 Hz on. Elastic modes of the dashboard are found above 60 Hz. Altogether 57 eigenfrequencies below 200 Hz are computed using this model. For a whole vehicle body many more modes are known in this frequency range. Herein, most of these local mode shapes are excluded when the substructure matrices are created.

The harmonic analysis is carried out by a modal superposition for the structure. The sound pressure level is calculated in the postprocessor by applying acoustic influence coefficients. A frequency step size of two Hertz is used. In spite of the large number of structural modes this stepping is found to be sufficient and efficient for the dashboard model.

The noise transfer function of the original and the initial model coincide up to about 50 Hz, Fig. 4. Most likely, this is subject to global vibration modes at lower frequencies. These global modes govern the elastic vibrations of the dashboard. The little difference in the geometry of the two models does not result in significant

global stiffness modification. For increasing frequencies, small differences of both models – the initial model is smoother – produce different local mode shapes. Consequently, above 50 Hz both functions show small differences where the general characteristics are the same for both up to about 150 Hz. Above that the local differences between both models lead to significant deviations of their noise transfer functions. These differences are subject to certain homogenizations where local shapes in the original model could not be transferred to the geometry based model. Moreover, the vibration mode shapes in the frequency domain above are more and more dominated by local loops of oscillation. These local vibration modes are much more sensitive to geometric parameters of the shell than the globally governed mode shapes which are essentially dominated by the remaining body.

5
Specification of objective function

In the optimization process we aim on decreasing booming noise. For this reason, the objective function is chosen to decrease sound pressure level peaks more than lower level domains. An objective function that can meet this requirement is given by (22) and (23) of Part I of this paper that are equivalent to

$$F = \frac{1}{f_{\max} - f_{\min}} \int_{f_{\min}}^{f_{\max}} \Phi\left\{p_{\mathrm{L}}(f)\right\} \,\mathrm{d}f\,,$$

$$\Phi\left\{p_{\mathrm{L}}\right\} = \begin{cases} \left(p_{\mathrm{L}} - p_{\mathrm{Ref}}\right)^n & \text{for} \quad p_{\mathrm{L}} > p_{\mathrm{Ref}} \\ 0 & \text{for} \quad p_{\mathrm{L}} \le p_{\mathrm{Ref}}. \end{cases} \tag{4}$$

It was a requirement to analyse the frequency range up to $f_{\max} = 200$ Hz. Certain permutations of the parameters $f_{\min}, p_{\mathrm{Ref}}$ and n provide six functions F_k being defined by the following combinations:

- F_1 : $f_{\min} = 0$ $p_{\mathrm{Ref}} = 0$ $n = 1$
- F_2 : $f_{\min} = 0$ $p_{\mathrm{Ref}} = 0$ $n = 2$
- F_3 : $f_{\min} = 24\,\mathrm{Hz}$ $p_{\mathrm{Ref}} = 0$ $n = 1$
- F_4 : $f_{\min} = 24\,\mathrm{Hz}$ $p_{\mathrm{Ref}} = 0$ $n = 2$
- F_5 : $f_{\min} = 24\,\mathrm{Hz}$ $p_{\mathrm{Ref}} = 76\,\mathrm{dB}$ $n = 1$
- F_6 : $f_{\min} = 24\,\mathrm{Hz}$ $p_{\mathrm{Ref}} = 76\,\mathrm{dB}$ $n = 2$

The choice of $f_{\min} = 24$ Hz and $p_{\mathrm{Ref}} = 76$ dB is based on the noise transfer functions Fig. 4 whereas the starting frequency of $f_{\min} = 24$ Hz additionally results from the parameter study being presented next, Fig. 5. Deviations between the different noise transfer functions can be observed from 24 Hz on.

For all optimization steps, F_6 was used as the objective function. However, the values of the five other func-

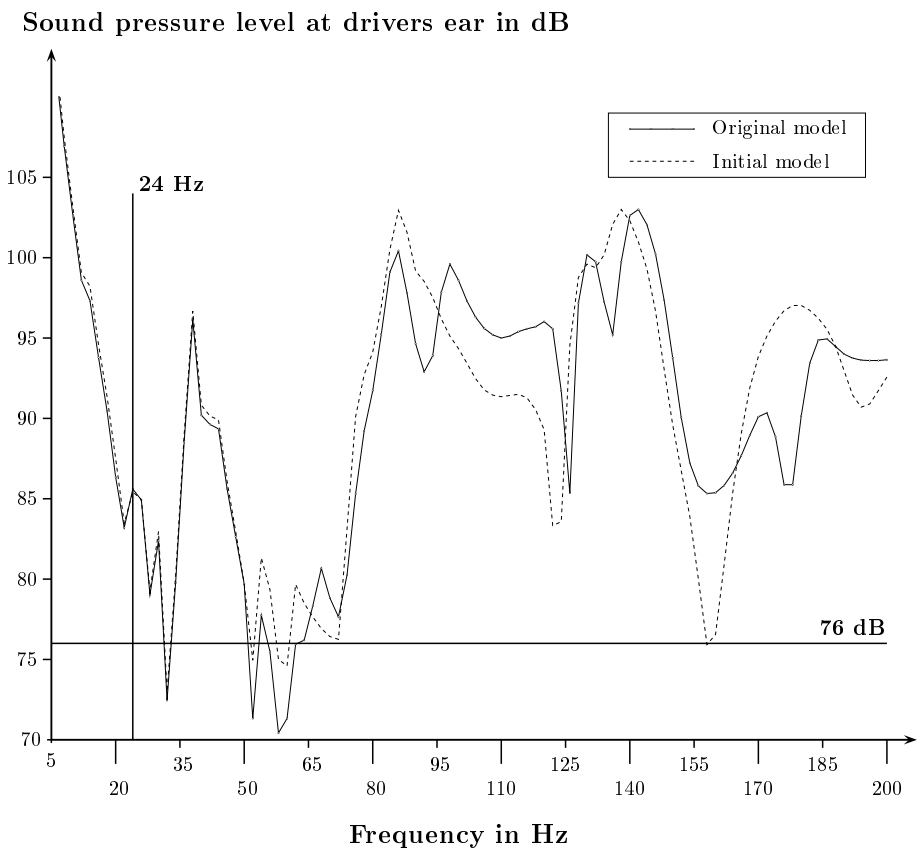

Fig. 4 Comparison of noise transfer functions of *original* and *initial* model

tions are provided as well. This may be useful for comparisons between the different objective functions.

6
Parameter study: fictitious stiffening

As former studies mostly provided a significant reduction of radiation by structural stiffening (cf. Marburg *et al.* 1997a,b), a fictitious stiffening is applied to study the noise transfer function modification with respect to Young's modulus. Objective of this study is to investigate whether a stiffening generally supplies a decrease of the noise transfer function. If so, this might be a strategy for optimization from an engineering point of view.

For this parameter study, the Young's modulus of all shell elements was multiplied by a scalar factor c in the range of $0.1 \leq c \leq 100$.

Recalling (28) of Part I

$$p_{\mathrm{L}}(\omega) = 20 \log_{10} \left(\frac{\left| i\omega \mathbf{b}^T(\omega) \mathbf{N} \mathbf{A}^{-1}(\omega, \boldsymbol{\vartheta}) \mathbf{f}(\omega) \right|}{p_0} \right), \qquad (5)$$

it is obvious that a stiff structure that supplies great matrix elements of A provides a low sound pressure level p_{L}. Furthermore, A is the only term that depends on the parameter set $\boldsymbol{\vartheta}$. On the other hand, we consider dynamic processes in a restricted frequency range. There, we may expect opposite effects in certain cases.

Now, the parameter under consideration is Young's modulus. It can be written as a constant factor of the static stiffness matrix $\mathbf{K}$ that is related to the dynamic stiffness matrix as given in (3) of Part I

$$\mathbf{A}(\omega) = \mathbf{K} + i\omega\mathbf{B} - \omega^2\mathbf{M}\,. \qquad (6)$$

If the dynamic stiffness matrix is dominated by its static part what especially occurs for low frequencies, an increase of Young's modulus will result in a decrease of the noise transfer function, (6). For higher frequencies, especially for frequencies above the first eigenfrequency this conclusion may become invalid. In this case, the model is not supported anywhere. Consequently, one cannot be sure that a stiffening will decrease the noise transfer function in the considered frequency range.

Table 1 shows that a decrease of the Young's modulus by factor ten results in a decrease of all objective functions. This effect can be explained by Fig. 5. It is observed that the stiffer original model has higher sound pressure level values in the upper frequency range, e.g. above

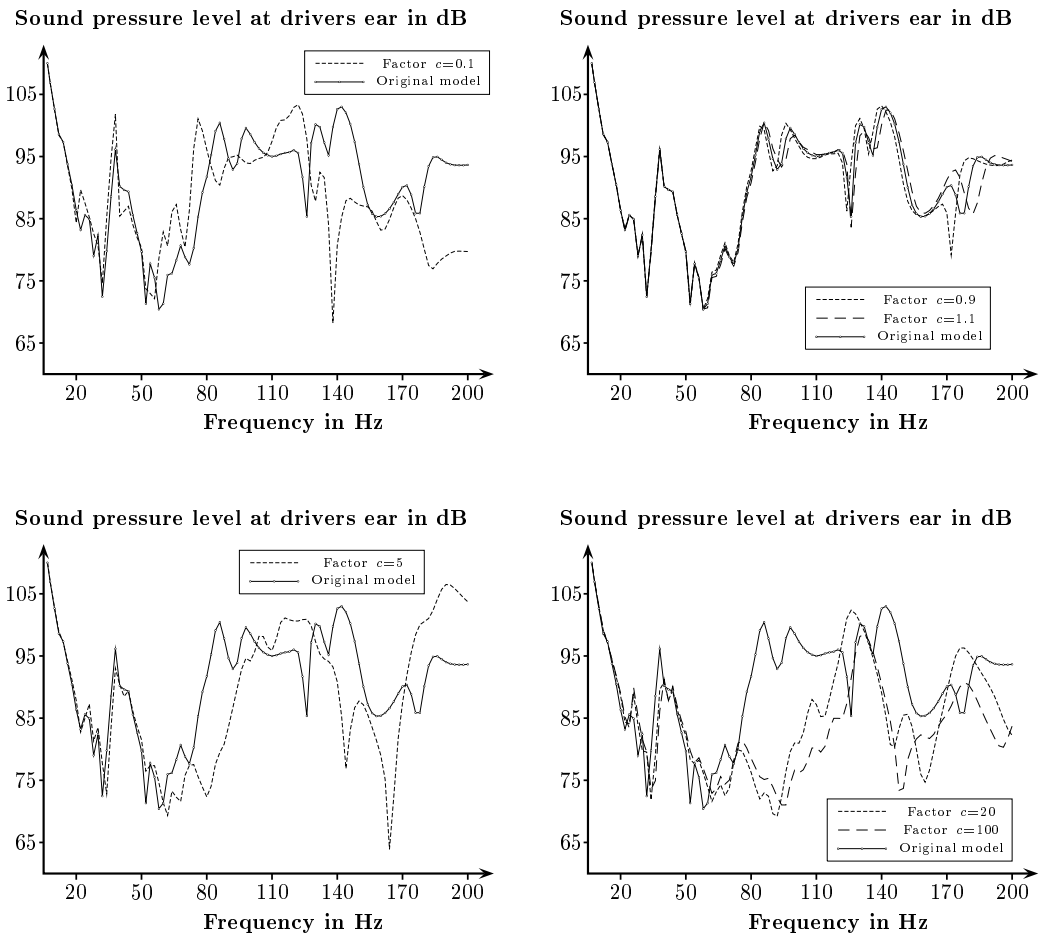

Fig. 5 Noise transfer functions of *original* model and those of a stiffened by modified Young's moduli

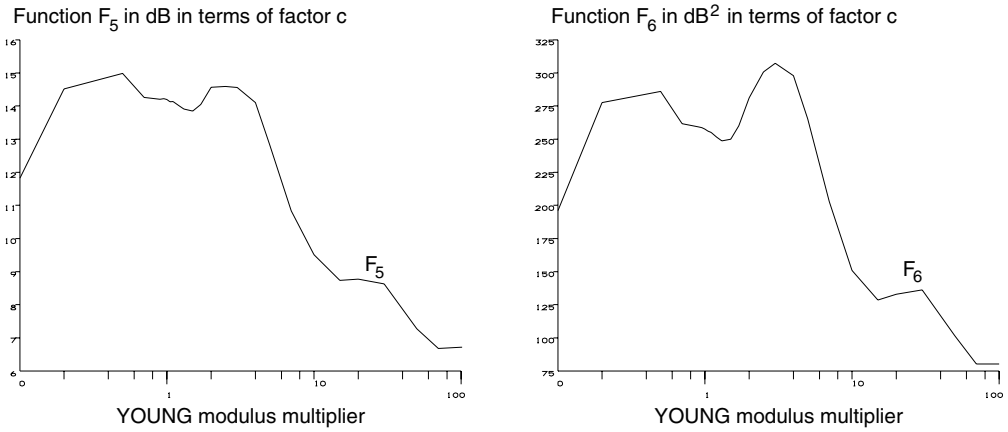

Fig. 6 Dependence of objective functions (5) and (6) in terms of a modified Young's modulus of dashboard

120 Hz where lower values are found for lower frequencies, especially between 50 and 80 Hz. Lower amplitudes in the low frequency range may be subject to a higher resistance of the shell structure. Higher sound pressure levels at higher frequencies can be subject to more global vibration modes whereas a softer structure allows more local vibration modes. The effects may also be explained by the above considerations on the stiffness matrices. Obviously, for frequencies below 80 Hz the dynamic stiffness matrix (case: $c = 1$) is dominated by its static part. Hence, the sound pressure is increased if the stiffness is decreased. This corresponds to a sensitivity analysis provided by a small modification of Young' modulus by factor 0.9, see also Fig. 5.

A similar behaviour can be observed for factors greater than 1.0 as can also be found in Fig. 5. In particular, the steep ascent between 70 and 80 Hz in the noise transfer function of the original dashboard is shifted to higher frequencies. It can further be seen that below 25 Hz hardly any changes in the noise transfer function occur. That is the major reason of the choice of 24 Hz as a lower bound (frequency step size 2 Hz). Again, one can notice a frequency range where the dynamic stiffness matrix is most likely dominated by its static part. This frequency range increases up to 130 Hz for a factor of $c = 100$.

An additional remarkable observation is that small modifications of the parameter result in significant differences of the sound pressure level above 150 Hz. This has been discussed in Sect. 4.

Finally, we point out to Fig. 6 showing the functions F_5 and F_6 over the Young's modulus multiplier. This is another reflection of the above discussed items. In general, both functions behave similarly. However, F_6 appears more distinctive than F_5.

Table 1 Values of six objective functions in terms of Young's modulus multiplier

	Objective function F_k					
	F_1	F_2	F_3	F_4	F_5	F_6
factor	[dB]	[dB^2]	[dB]	[dB^2]	[dB]	[dB^2]
0.1	89.23	8059	87.61	7738	11.82	196.0
0.5	92.08	8571	90.85	8319	14.98	286.0
0.9	91.32	8432	90.00	8164	14.21	259.3
original	*91.31*	*8429*	*89.98*	*8160*	*14.20*	*257.6*
1.1	91.24	8416	89.91	8146	14.13	255.2
1.3	91.02	8378	89.67	8103	13.91	248.7
2.0	91.58	8492	90.29	8231	14.57	281.3
3.0	91.51	8506	90.21	8244	14.56	307.4
5.0	89.79	8208	88.25	7907	12.83	265.2
7.0	87.91	7870	86.13	7524	10.84	203.0
10.0	86.83	7657	84.90	7283	9.51	150.9
15.0	86.17	7537	84.15	7146	8.74	128.7
20.0	86.21	7547	84.19	7156	8.77	132.9
30.0	85.93	7509	83.87	7113	8.63	136.2
50.0	85.02	7338	82.84	6919	7.27	101.5
100.0	84.55	7246	82.30	6815	6.72	80.2

7 Description of parameters

A total of 44 parameters is used in the optimization process. As parameters enable modification of keypoints in normal direction, they can be mapped to keypoint numbers. Consequently, the parameters are indicated by numbers in the *line* model in Fig. 7.

Comparison between Figs. 7 and 3 shows that 24 *keypoints* with parametrically described normal coordinates are located above the horizontal welding point line and 20 *keypoints* below.

No parameters are put in the lower right part or in the whole spherical right part of this dashboard symmetry half. The first corresponds to the preposition that welding points must not be modified. As they are situated very close together only very local modification would be possible. It was unlikely that these very local modifications could essentially improve the vibrational behaviour. However, they would complicate the problem. The *key-*

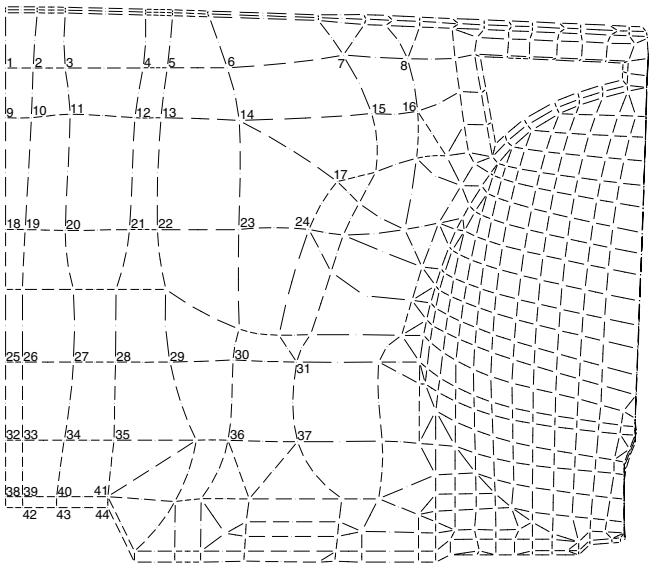

Fig. 7 Line model of dashboard symmetry half, indication of *keypoints* with parametric position

points at the wheel casing have got the same coordinates as the nodes of the original shell structure. Consequently, the line and the area topology is the same as that of the element topology in the original model. This topology is kept since the noise transfer function appears most insensitive with respect to geometry modifications in the stiff wheel casing shell domain.

The choice of these parameters has the advantage that all 44 parameters are of the same dimension. They all describe positions of *keypoints* directly and may vary in a range of

$$-10\,\mathrm{mm} \le \vartheta_k \le +10\,\mathrm{mm}\,, \qquad k = 1, 2, \ldots, 44\,. \tag{7}$$

Often, *lines* are created by connecting several points using cubic splines. So, in certain cases it may happen that although all parameters are modified within the above mentioned interval, a higher maximum change of geometry in the finite element model is observed. However, the feasible design range may be considered an approximate one and one or two percent overshoots could be allowed for this practical problem.

The dashboard is to be optimized in the frequency range up to 200 Hz. At this frequency the fluid wavelength is 1.7 m. A comparison to the maximum 10 mm modification allows to apply (24) of Part I of this paper

$$\frac{\partial \mathbf{b}}{\partial \boldsymbol{\vartheta}} = \mathbf{0}\,. \tag{8}$$

This is indicating that the influence coefficients are independent of the design parameters.

8 Optimized structure

Being aware that the total of 44 is a huge number of parameters and further taking into account the strongly nonlinear nature of the objective function with respect to every single parameter we can be sure that we will not find the optimum. However, for technical requirements a significant improvement of the objective function in a certain period of time is more important than a long or almost infinite search for the global minimum.

The semianalytic sensitivity analysis described in part one of this paper is only used for the first few steps in the optimization process. In these cases the reference sound pressure level is decreased below the lowest value, in most cases 70 dB. It is then necessary to control the optimization process manually. Later, p_{Ref} is increased to 76 dB as indicated in Sect. 5. As mentioned before, the C^1-continuity of the objective function is then lost. On the other hand, low level domains do not influence the objective function. Furthermore, a high reference level improves the conditioning of the objective function to decrease maxima, a target that we are aiming on here.

The noise transfer function of the optimized structure is compared to those of the initial and the original models in Fig. 8. Hardly any changes may be observed for frequencies lower than 50 Hz. In the continuing part, it is slightly increased whereas the peaks at 86, 98, 130 and 142 Hz are all decreased significantly by about eight decibel. As expected and admitted, the sound pressure level is increased for low level regions, as for example between 50 and 80 Hz or between 150 and 180 Hz.

Table 2 supplies the values of functions F_1 to F_6 for the original, the initial and the optimized model. Additionally, the square root of F_6 is listed to enable a comparison between F_5 and F_6, the simple average and the square mean value. Comparing the original and the optimized model, the improvement for F_1 is of about 2.5 dB,

Table 2 Values of six possible objective functions for original, initial and optimized dashboard model, objective function used in the optimization process: F_6

	Objective function						
model	F_1 [dB]	F_2 [dB^2]	F_3 [dB]	F_4 [dB^2]	F_5 [dB]	F_6 [dB^2]	$\sqrt{F_6}$ [dB]
original	91.31	8429	89.98	8160	14.20	257.6	16.05
initial	91.34	8437	89.94	8154	14.02	258.2	16.07
optimized	88.80	7954	87.09	7612	11.18	149.6	12.23

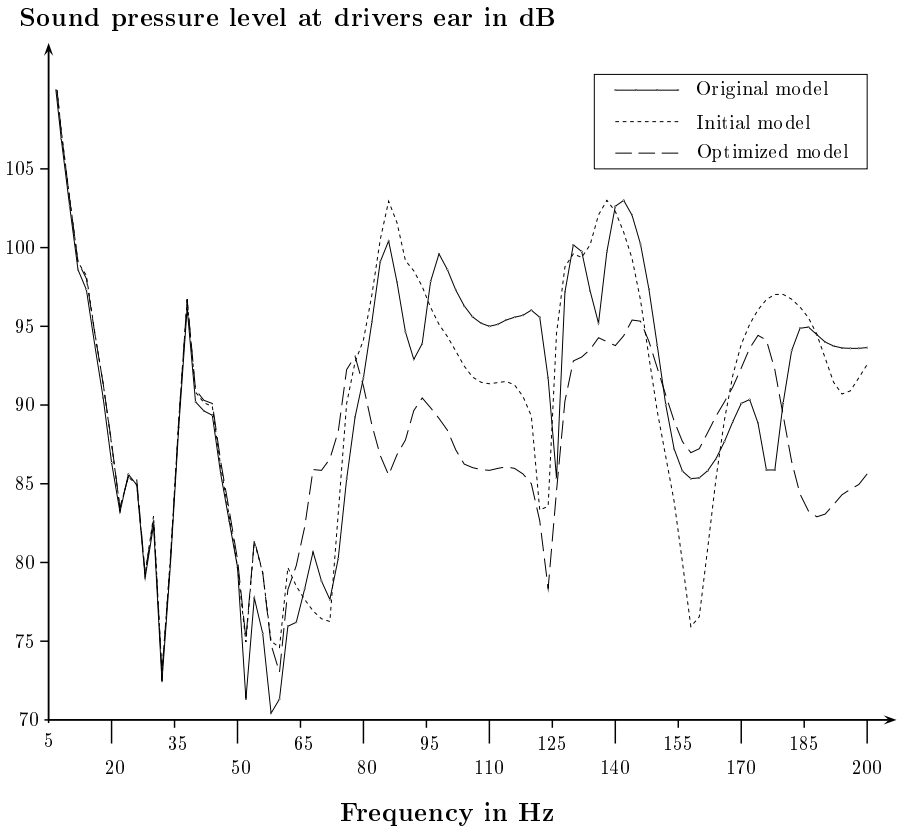

Fig. 8 Comparison of noise transfer functions of *original*, *initial* and optimized models

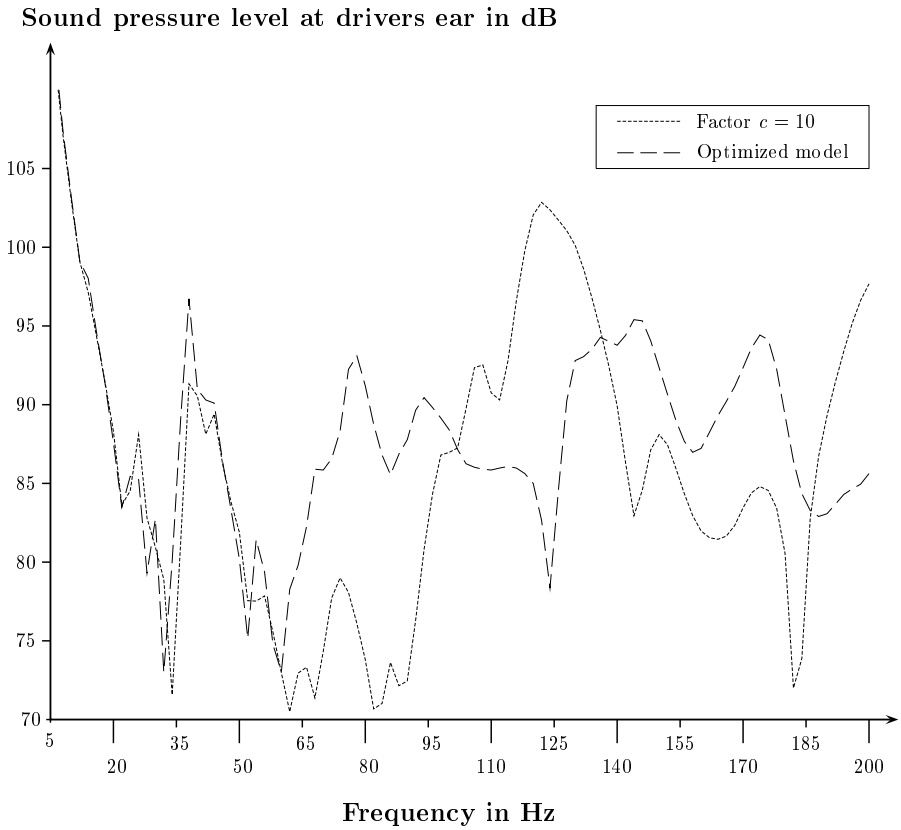

Fig. 9 Comparison of noise transfer functions of *original* model with a ten times higher Young's modulus and the optimized structure

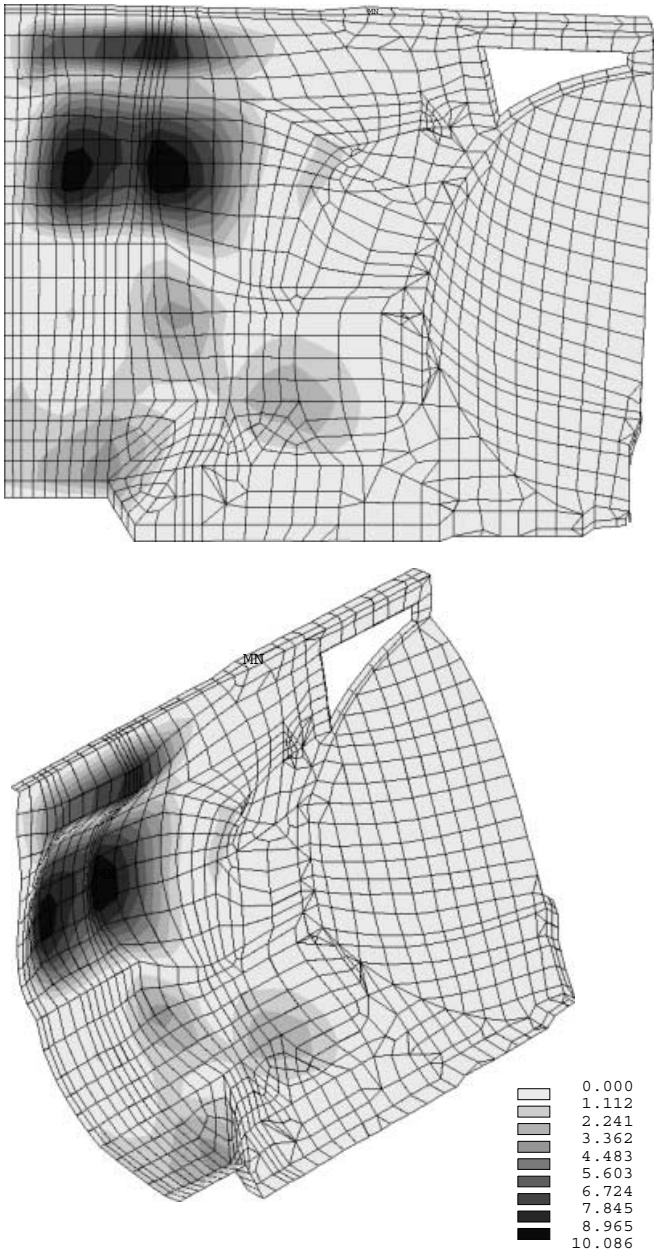

Fig. 10 Dashboard modification (scale in mm), horizontal bead in the upper part directing to the right front seat, two bulges below directing to the engine, little geometric changes in the lower part, viewpoint of upper picture: right front seat, viewpoint of lower picture: left front seat

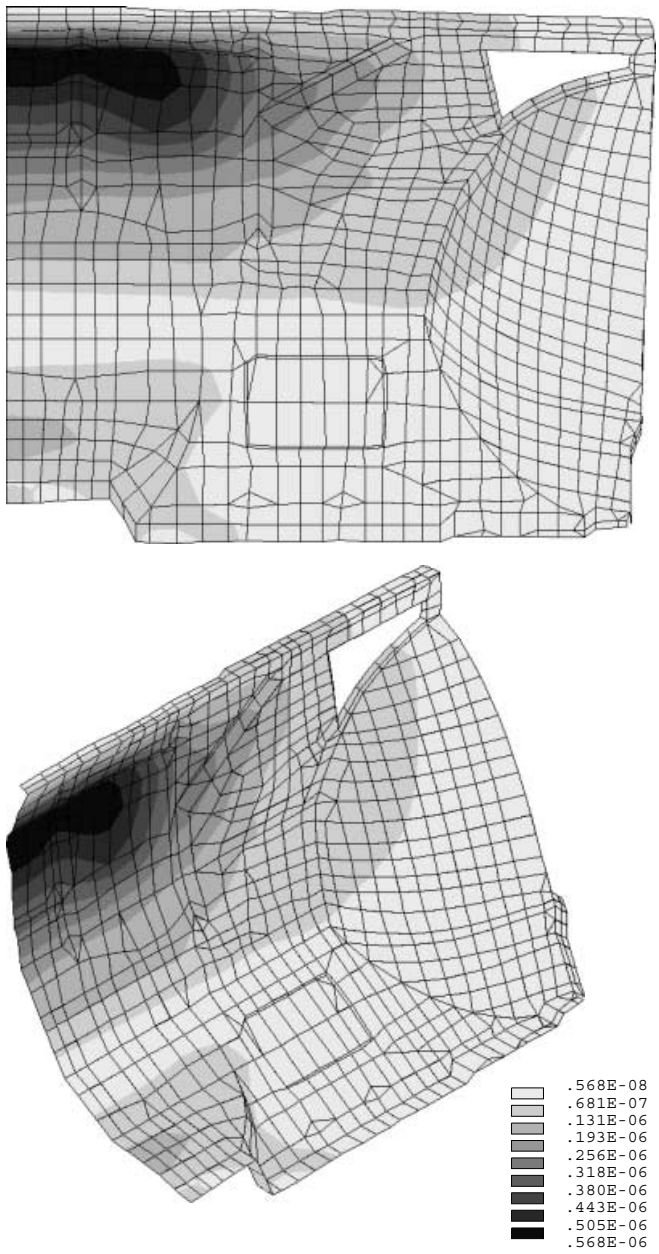

Fig. 11 Original dashboard vibration mode shape (Real part, displacement scale in mm), excitation at engine, frequency: 100 Hz, imaginary part: similar mode shape, one global loop of oscillation, viewpoint as in Fig. 10

for F_5 3.0 dB and for F_6 3.8 dB. This indicates that the optimization process essentially took advantage of the chosen objective function in the desired sense.

Finally, we want to compare the stiffened original model, factor $c = 10$, with the optimized one. The value of F_6 is about the same for both models. However, the difference in F_1 is 2.0 dB and in F_5 as much as 1.7 dB. The comparison of both noise transfer functions, Fig. 9, clarifies the differences. As explained before, the noise transfer function of the optimum fulfills the requirements of an average low sound pressure level with, if possible, all peaks of about the same size. The noise transfer function of the stiffened model shows wide ranges of low sound pressure levels. On the other hand, there is one peak that is about eight decibel higher than all peaks of the optimized dashboard (above 50 Hz). This peak covers a frequency range of virtually twenty Hertz.

The new geometry of the dashboard is illustrated in Fig. 10, which shows the geometric modification with respect to the initial model. Note, that this modification appears enlarged. It can be observed clearly, that the modifications essentially occur in the upper part of the dashboard whereas the lower part is changed very little.

The main structural elements of the modification consist of a nine millimeters deep horizontal bead in the direction of the right front seat and two ten millimeters deep bulges below. The latter ones are formed in the direction of the engine. It is mentioned that in the upper domain the *keypoint* positions at the symmetry line are not affected by the optimization procedure. The small modifications in the lower part include the *keypoint* positions on the symmetry line.

Finally, we consider mode shapes and spectral properties. This might help the reader to understand the optimization process from an engineering point of view. Marburg *et al.* (1997a,b) increased the dynamic stiffness during the optimization process. The dynamic stiffness was represented by the number of eigenfrequencies below a certain upper limit. The listing in Table 3 consists of these numbers of eigenfrequencies below certain frequency limits. Hardly any differences between the original model and the optimized one can be observed. Obviously, the initial model is more pliable than the other two. Most likely, this is subject to the homogenization that was applied when the initial model was created. Similar explanations apply for the column of the 80th eigenfrequency. Hence, one may conclude that the dynamic stiffness has hardly been increased during the optimization process.

Table 3 Number of eigenfrequencies below certain upper limits and 80th eigenfrequency (EF) for the original, the initial and the optimized models

	Number of eigenfrequencies below						80th
	50	100	150	200	250	300	EF
model	Hz	Hz	Hz	Hz	Hz	Hz	[Hz]
original	15	31	47	57	65	77	309
initial	15	32	48	59	69	81	294
optimized	15	31	47	57	65	76	313

Consequently, the improvement of the acoustic behaviour must be due to modified vibration mode shapes. Indeed, it is detected, that these mode shapes do essentially change during the optimization process. One example may be the vibration mode at 100 Hz. This frequency is arbitrarily chosen as one frequency for which the noise transfer function could be decreased by some decibel. Figure 11 shows the mode shape (real part) for the original model. One can easily recognize one global oscillation loop that causes an unfavourable acoustic behaviour. In contrast to this global loop, Fig. 12 shows the vibration mode (real part) for the same frequency of the optimized model. Now, we obtain two major oscillation loops in different directions. Similar to a dipole, these two loops cause a near field but mainly erase each other in the far field. It is mentioned, that the maximum displacement has been increased in the optimized model. Since this may be considered as an unwanted effect, we recommend to control the average maximum displacement

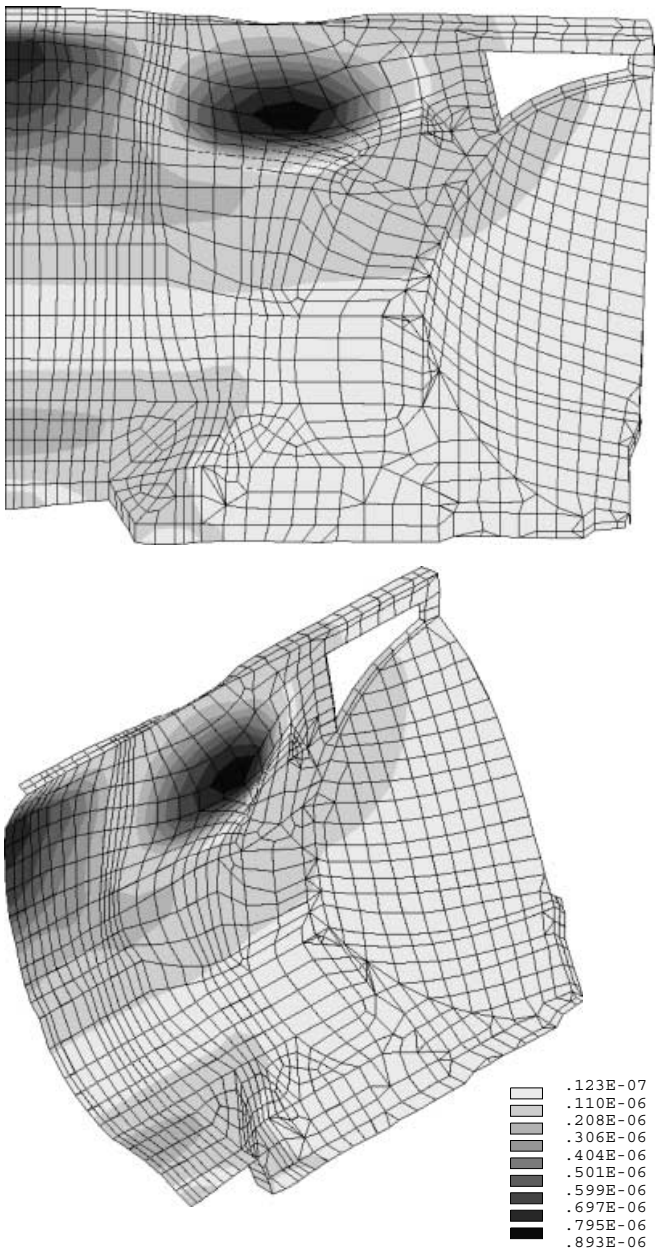

Fig. 12 Optimized dashboard vibration mode shape (Real part, displacement scale in mm), excitation at engine, frequency: 100 Hz, imaginary part: similar mode shape, two loops of oscillation that extinguish each other at the driver's ear, viewpoint as in Fig. 10

during the optimization process. In general, the search for optimized vibration mode shapes does most likely account for the optimizing strategy from an engineering point of view.

9 Discussion of results and conclusions

Although the optimization strategy does not end up in a stiffening as observed in former investigations, the decrease of the noise transfer function as well as of the

objective function F_6 may be considered as a significant improvement again. It is true that the improvement is not as high as that reported by Hambric (1995), Marburg *et al.* (1997a) or Pal and Hagiwara (1994). On the other hand, geometric modifications of $\pm$ 10 mm are very small compared to the width and the height of the structure. The mass of the structure remains more or less unchanged.

Unfortunately, it is impossible to compare the computational results for the component model neither by computing the noise transfer function of the entire body structure nor by experimental measurements. For this reason, some critical aspects will be discussed in the following.

The fact that the optimization results are essentially based on modified vibration mode shapes indicates that the optimization method requires realistic and reliably predicting models. This applies for the structure as well as for the fluid model. The entire symmetry half of the body structure did not include parts of the typical trim elements like seats. Seats were also excluded from the fluid model as well as the driver himself. The uniform boundary admittance is certainly more realistic than no fluid damping. Obviously, determination of realistic spatially distributed boundary admittance values seems to be an important task to accomplish the entire structural-acoustic model of the total vehicle. In that case, there would be a number of additional aspects that had to be taken into account, i.e. damping by poroelastic layers. Consideration of these additional parameters most likely provides further noise level reductions since less sound is radiated and absorption can be increased.

The optimized structure reduces the sound pressure at the driver's ear. However, it should be discussed what happens for other configurations of passengers in the car, for other positions of the driver or his ear. These cases have not been considered in this paper. If one intends to include several passenger configurations as well as different driver positions, suitable concepts of multicriteria optimization are required. On the other hand, for low frequency problems loop areas of oscillation like those in Fig. 12 really do appear as dipole elements since the corresponding influence coefficients on this (vibrating) surface are all of the same order. This is subject to the wavelength (3.4 m for 100 Hz) in comparison with the size of the vibrating part of that structure. These proportions are preserved for different passenger positions in the car so that extinguishing loops will effectuate similarly for different positions. On the other hand, the level of the influence coefficients might be different for different positions. Hence, large amplitude structural vibrations may be shifted into a frequency range with lower acoustic influence coefficients. This could possibly result in a high sound pressure peak for another passenger at this frequency range. Thus, detailed investigations of these points may be useful.

Optimization at a component model suitably reduces computational costs. On the other hand, especially for higher frequencies, the success of the method in the entire vehicle body is not guaranteed. This failure may occur in case of certain interference phenomena, for example if panel vibrations of two surfaces in the original model extinguish each other. However, these phenomena usually apply for certain frequency ranges only. Solution of this problem may be achieved by optimization of the entire body with modification of just one panel after each other. Because this will be computationally too expensive, an iterative approach can be tried. An approach like this should include the technique that was presented in this paper for the dashboard. After finishing one panel the consequences on the entire body are to be tested. Then, the process is repeated for another panel.

Reliable models for prediction of the acoustic behaviour provided, the optimization of shell structure geometries can set free great resources to design for silence.

Acknowledgements The financial support of the Ford-Werke AG Köln, Germany, is gratefully acknowledged. We kindly appreciate Mr. G. Dödlbacher and Dr. G. Booz of the Ford-Werke AG for the many stimulating talks and helping instructions in connection with this work. Dr. Booz provided the superelement matrices. Furthermore, the authors wish to acknowledge that the SGI ORIGIN 2000 at the Zentrum für Hochleistungsrechnen (ZHR) of the Technische Universität Dresden was used to carry out parts of computational work. Finally, we thank Francois Lautel from the Ecole Supérieure de Mécanique de Marseille for his part of computation.

References

Christensen, S.T.; Olhoff, N. 1998: Shape optimization of a loudspeaker diaphragm with respect to sound directivity properties. *Control Cybernetics* **27**, 177–198

Christensen, S.T.; Sorokin, S.V.; Olhoff, N. 1998: On analysis and optimization in structural acoustics. Part I: problem formulation and solution techniques. *Struct. Optim.* **16**, 83–95

Flanigan, D.L.; Borders, S.G. 1984: Application of acoustic modeling methods for vehicle boom analysis. *SAE-paper 840744*

Giebeler, W.-R.; Booz, G. 1994: Akustisches Verhalten als Zielvorgabe in der Karosserieentwicklung. *Berechnung und Simulation im Fahrzeugbau*, pp. 237–252. VDI–Report 1153

Hagiwara, I.; Ma, Z.-D.; Arai, A.; Nagabuchi, K. 1991: Reduction of vehicle interior noise using structural-acoustic sensitivity analysis methods. *SAE Technical Paper Series No. 910208*

Hambric, S.A. 1995: Approximation techniques for broad–band acoustic radiated noise design optimization problems. *J. Vib. Acous.* **117**, 136–144

Hambric, S.A. 1996: Sensitivity calculations for broad–band acoustic radiated noise design optimization problems. *J. Vib. Acous.* **118**, 529–532

Ishiyama, S.-I.; Imai, M.; Maruyama,S.-I.; Ido, H.; Sugiura, N. Suzuki, S. 1988: The application of ACOUST/BOOM – A noise level prediction and reduction code. *SAE–paper 880910*, pp. 195–205

Kitamura, H.; Sano, M.; Fukushima, M.; Yagi, T.; Furuyama, M. 1990: Use of structural-acoustic coupling analysis to improve the acoustic characteristics of the vehicle body. *SAE-paper 905216*

Marburg, S.; Hardtke, H.-J. 1999: A study on the acoustic boundary admittance. Determination, results and consequences. *Engrg. Anal. Boundary Elements* **23**, 737–744

Marburg, S.; Hardtke, H.-J.; Schmidt, R.; Pawandenat, D. 1997a: An application of the concept of acoustic influence coefficients for the optimization of a vehicle roof. *Engrg. Anal. Boundary Elements* **20**, 305–310

Marburg, S.; Hardtke, H.-J.; Schmidt, R.; Pawandenat, D. 1997b: Design optimization of a vehicle panel with respect to cabin noise problems. *Proc. NAFEMS World-Congr.*, pp. 885–896 Stuttgart

Mühlmeier, M.; Kumbein, T.; Vogler, N. 1994: Identifikation und Reduzierung der Flächenbeteiligungen am niederfrequenten Innenraumgeräusch. *Berechnung und Simulation im Fahrzeugbau*, pp. 221–235. VDI–Report 1153

Pal, C.; Hagiwara, I. 1994: Optimization of noise level reduction by truncated modal coupled structural-acoustic sensitivity analysis. *JSME Int. J., Series C* **37**, 246–251

Yamazaki, I.; Inoue, T. 1989: An application of structural-acoustic coupling analysis to boom noise. *SAE-paper 891966*

Zienkiewicz, O.C. 1977: *The finite element method*, 3rd. edn. Berkshire: McGraw Hill